Study of the stability under in vitro physiological conditions of surface silanized equimolar HfNbTaTiZr high-entropy alloy: A first step toward bio-implant applications

M. Gueye, S. Ammar-Merah, S. Nowak, P. Decorse, A. Chevillot-Biraud, L. Perrière, J.P. Couzinie, I. Guillot, G. Dirras

Version of Record: https://www.sciencedirect.com/science/article/pii/S0257897220300438
Manuscript_9b75193d11b9de0000e644cc6d9cb07c

Study of the stability under in vitro physiological conditions of surface silanized equimolar HfNbTaTiZr high-entropy alloy: a first step toward bio-implant applications

M. Gueye[1,2,3], S. Ammar-Merah[2,*], S. Nowak[2], P. Decorse[2], A. Chevillot-Biraud[2], L. Perrière[3], J. P. Couzinie[3], I. Guillot[3], G. Dirras[1,*]

[1.] Université Paris 13, Sorbonne Paris Cité, CNRS, LSPM (UPR 3407) 99 avenue JB Clément, 94430 Villetaneuse, France.

[2.] Université Paris Diderot, Sorbonne Paris Cité, CNRS, ITODYS (UMR-7086), 15 rue JA de Baïf, 75205 Paris, France.

[3.] Université Paris Est Creteil, CNRS, ICMPE (UMR 7182), 2-8 rue Henri Dunant, 94320 Thiais, France.

* Corresponding author: ammarmer@univ-paris-diderot.fr, dirras@univ-paris13.fr

ABSTRACT

A methodology of surface chemical functionalization of equimolar HfNbTaTiZr high-entropy alloy (HEA) is presented herein. The aim is to improve the biocompatibility of this material for its application as bio-implants. X-ray Photoelectron Spectroscopy (XPS) showed that air or aqueous oxidation of HfNbTaTiZr induced the formation at its surface of unmixed monometallic oxides: TiO_2, Nb_2O_3, ZrO_2, Hf_2O_3, and Ta_2O_5. Besides, it was observed that short (2 hours) mild aqueous oxidation (without H_2O_2) retains the surface stoichiometry of these elements compared to a more aggressive one (with H_2O_2). The mild oxidation was retained to form a sol-gel chemistry platform for HfNbTaTiZr surface silanization. In practice, the oxidized HfNbTaTiZr surface was reacted with 2-methoxy [(polyethyleneoxy)$_{6–9}$ propyl] trimethoxysilane (MPTMS), dissolved in distilled ethanol, under an inert atmosphere. Both, the precursor concentration and the reaction time, were varied to define the optimized operating conditions. Infrared spectroscopy performed on all prepared samples, within an attenuated total reflectance (ATR) sampling configuration, evidenced the well-known vibrational signatures of Si-O and C-H bonds at 1100 cm^{-1} and 2980 cm^{-1}, respectively,

confirming silane grafting, and showed that the intensity of these bands increases when the reaction time and/or the siloxane precursor concentration increase. Moreover, XPS showed that a reaction time of 48 hours is required to completely cover the alloy surface with an organic layer thickness larger than the XPS analysis depth. Finally, as a preliminary study, mildly oxidized alloy and the grafted one for a reaction time of 48 hours were contacted to a Phosphate-Buffered Saline (PBS) solution and a standard Nutrient Mixture for cell cultures, the well-known Dulbecco's Modified Eagle Medium (DMEM), up to one month to check their chemical stability. None metal release was evidenced for the treated sample highlighting the importance of surface processing before any bio-implant use.

KEYWORDS

High entropy alloy (HE); Surface functionalization; Sol-gel chemistry; X-ray Photoelectron Spectroscopy (XPS); Chemical stability under in-vitro physiological conditions.

1. INTRODUCTION

A growing need for a new generation of metallic materials with superior biocompatibility and adequate mechanical properties (strength-ductility synergy, fatigue endurance, Young modulus close to that of bone) is emerging. The aging of the population in our modern societies and the increased risk of bone disease or bone accident is continuously growing and the development of such materials with a long life cycle time is a significant public health issue. Indeed, it is essential to tailor advanced structural materials allowing a net extent of the revision surgery period than the actual 10 years limit [1,2]. According to recent United Nations reports, the population of the over 60 age group is overgrowing, and the ratio of older people is expected to increase by 45% as of 2050 [3]. So with such a rising human life expectancy, a period of ten years is a short time.

Up to now, the primary strategy for optimizing the mechanical performances of metallic materials has long been based on the adjustment of the chemical composition and the microstructure of conventional Ti alloys. Compounds like Ti6Al4V and TiZrNb emerged as the best materials for bio-implants [4]. While the former displays a Young modulus (E) of about 110 GPa [4], higher than that of bone (4-30 GPa [5,6]), the latter can exhibit E ~ 14 GPa (Ti19Nb14Zr) [7] but perfectible mechanical properties compared to the widely used Ti6Al4V.

Moreover, if the TiZrNb alloys, contain less-toxic elements, the Ti6Al4V ones do not. The risk of Al or V release is real, and the toxicity of these elements is acute [8]. It was for instance established that debris particles of worn Ti6Al4V could induce the release of inflammatory mediators affecting the tissues surrounding the prosthesis and cause osteolysis [9]. Therefore, even if Ti6Al4V is still largely used, the TiZrNb-based alloys are becoming better candidates, particularly if their mechanical properties can be still improved.

The proximity of the Young modulus of the implant material to that of bone is not the unique criteria to avoid implant rejection or failure. It is now assumed that implant failure over the time can be caused by different factors [10-13]: i) a mismatch in modulus of elasticity between bone and implant, ii) a low fracture toughness in relation with a low fatigue strength, iii) a wear resistance, iv) a corrosion resistance and v) a non-bonding with the surrounding tissue leading to fibrous encapsulation and/or inflammation and then implant rejection. So, among all these factors, the "Young modulus" criteria remains still essential. Indeed, if the implant material has a higher stiffness than bone, it induces a stress shielding effect [13]. In practice, it prevents the transfer of the needed stress to adjacent bone, resulting in bone resorption around the implant and, consequently, the implant loosening. So, even if Ti6Al4V is still primarily used, the TiZrNb-based alloys are becoming better candidates, notably if their mechanical properties can be still improved.

Recently, the concept of high entropy alloys (HEAs), formed by mixing equal or relatively large proportions of five or more elements, instead of one or two like in conventional alloys, brings real hopes [14-18]. They exhibit specific strength and corrosion resistance together with Young's modulus very close to that of bone [15]. So, therefore, HEAs based on TiZrNb alloy systems could be a smart and elegant materials solution for bio-implant applications.

To date only (HfNbTaTiZr)C and (HfNbTaTiZr)N coating of Ti6Al4V alloys have been considered, and preliminary results have shown that hardness, friction performance, and

wear–corrosion resistance of the resulting composites are significantly enhanced compared to pristine Ti6Al4V [19] or compared to more conventional carbide, nitride or carbonitride coating [20-22]. Moreover, osteoblast cells contacted with these composites have exhibited better adherence, remaining in life over a minimum of 72 hours [19]. Contrariwise to their carbide or nitride counterparts, to date, reports on the use of bulk HfNbTaTiZr as implant materials are missing. Results exist, but they mainly concern alloys with a composition close to that of HEAs but not classified as HEAs, deriving from β titanium alloys composition, in particular, Ta and/or Mo derivatives of TiZrNb family [23,24]. These alloys are seriously considered as bio-implant material alternatives when coated by a thin ceramic (TiN, TiO_2…) or polymer (PLGA…) layer for the improvement of their biocompatibility. From this family, maybe the closest alloy to the HEA composition is those of the TiZrNbTaMo [18,25-27] or TiZrNbCrMo [17] families. These data confirm their excellent corrosion resistance in phosphate-buffered saline (PBS) and other mimetic physiological media. They also evidence high compressive yield strength and large deformation before failure (for instance, up to 1300 MPa and 6 %, respectively, in the case of the equimolar TiNbTaZrMo alloy [27]) better than those measured on their TiZrNb parent alloys. Unfortunately, the reported Young modulus for these compounds were found higher than those of bone (for instance around 153 GPa in the case of the equimolar TiNbTaZrMo alloy [27]), meaning that compositions closer to HfNbTaTiZr remain still required.

Adjusting the alloy's composition to equimolar HfNbTaTiZr, like in true HEAs, allowed decreasing the Young modulus value significantly, confirming the pertinence of this kind of HEA for the desired application. Indeed, low Young's modulus and high compressive yield strength values, ranging between 78 and 110 GPa [15,28] and 890 to 1015 MPa [15,28], respectively, were recently reported, depending on the alloy's processing conditions. For instance, fully recrystallized HfNbTaTiZr (grain size of 40 μm) displays an elastic modulus of 92 GPa, a

yield strength at 0.2% of 940 MPa, a sharp elastic to plastic transition and a uniform elongation larger than 15% and an ultimate tensile strength of 1090 MPa (tensile tests carried out under a strain rate of 10^{-4} s^{-1}) [29]. Moreover, these alloys exhibit usually significant ductility [30] and improved fatigue behavior [31], making them on the top of the most promising ones for bone substitution..

Surprisingly, despite these exciting mechanical properties, to the best of our knowledge, there is a lack of investigations on the biocompatibility of HfNbTaTiZr nor on their chemical functionalization in order to improve it, in terms of corrosion resistance and surface water wettability. This lack is mainly because Hf, Nb, Ta, Ti, and Zr elements are assumed to be non-toxic or at least less toxic than Al and V in Ti6Al4V [4,32]. Also, because metallurgists supposed that the biochemical properties of HfNbTaTiZr alloys must be similar to those of their constituting elements [4,33,34]. This is supported by the fact that the chemical nature of HfNbTaTiZr remains closer to that of β titanium alloys, which are already used in clinic [35].

So, we decided to investigate the effect of air and water oxidation of HfNbTaTiZr as well as the different steps of its chemical functionalization, to make it hydrophilic and more resistant to metal release when contacted to physiological media. Surface silanization was specifically chosen since it is one of the most used surface chemical treatments for bio-implants [36-39]. In practice, we applied a series of treatments on platelets of $1.0 \times 0.7 \times 0.1$ cm^3 in size: first, a mechanical polishing using different grades of polishing discs and leading to samples with different surface roughness, from very smooth to very rough; second, a controlled chemical oxidation in more or less aggressive chemical baths and third, a surface silanization by reacting the oxidized alloys with a PEGylated silane, the 2-methoxy [(polyethyleneoxy)6–9 propyl] trimethoxysilane (MPTMS), using sol-gel chemistry. This surface chemistry requires the presence of hydroxyl -OH groups on the surface of the reacting alloys. These groups are provided during the aqueous oxidation step. Finally, we demonstrated that this coating

prevents the alteration of the chemical surface composition when contacted, for a long time, with biomimetic media, like Phosphate-Buffered Saline (PBS) solution and/or standard Nutrient Mixture for cell cultures, promoting definitively silanized equimolar HfNbTaTiZr in the field of bio-implant technoloy.

2. EXPERIMENTAL

2.1. Chemicals products

$C_2H_2O_4$ oxalic acid and hydrogen peroxide H_2O_2 were obtained from Sigma Aldrich. Absolute ethanol was purchased from VWR Chemicals. Argon gas was from Air-Liquid. MPTMS and aminopropyl trimethoxysilane (APTMS) reagents were obtained from ALFA Chemistry.

2.2. Sample preparation

HfNbTaTiZr was prepared by melting techniques [40]. Raw metals were used in the form of slugs and wires with a purity exceeding 99.9 wt.-%. Arc melting was first used to prepare master alloys (Ti–Zr–Hf and Ta–Nb), each alloy being melted twice. The final mixture was then subsequently melted by an arc and by induction to grant a full dissolution of all the five elements. It was then shaped like an ingot of approximately 60 mm in length and 10 mm in diameter by arc melting. The ingot was then 75% rolled for a thickness of 1 mm and then annealed under helium flow at about 1050°C for 5 hrs before to be cut into platelets of 0.7×0.1 cm^2 in size. The chemical composition of the produced alloys was first confirmed before to continue its processing as well as its microstructure and its main mechanical properties [29]. The platelets were finally mechanically polished, leading to different surface roughness: unpolished and polished at 2000 and mirror grades.

2.3. Surface oxidation

All the produced platelets were cleaned in ethanol for 10 min by ultra-sonication and therefore immersed in three different aqueous oxidation baths for 2 hrs: 5% oxalic acid in

water (golden oxidation), 5% oxalic acid in 30% hydrogen peroxide (grey oxidation) or 5% oxalic acid in water followed in this case by a hydrothermal treatment at 80°C for 24 hrs in a solution made of 15 mL of H_2O_2 (30 %) and 15 mL of NaOH (10 M) (white oxidation). After rinsing in water and drying with pressurized argon, the platelets were calcined in air at 450°C for 30 min.

2.4. Silanization

MPTMS grafting was performed by sol-gel chemistry operating in distilled ethanol, at room temperature, and under an argon atmosphere, without stirring. Preliminary assays were performed by replacing MPTMS by APTMS (scheme 1), a more common and less expensive silane. We selected APTMS, as a test reagent, knowing that its reaction time will be shorter than that of MPTMS. It bears the same methoxy groups and leaves a terminal NH_2 group, which may serve as a specific signature, for grafting quantification. Obviously, we were expecting longer period of incubation to complete silanization reaction with the bulky Pegylated MPTMS reagent. For such oligomers, long reaction times are often required, even when they are introduced in a large excess into the reaction medium [41-42]. This due to the lack of contact between the surface hydroxyl groups and their borne alkoxysilane groups. PEG is in a random coil shape in bulk solution, and there is no driving force to adsorb to the surface [43,44]. So, in practice we defined more adapted operating conditions (Table 1):

Table 1: Main operating conditions used for the MPTMS silanization's process.

Series	Solvent	Temperature (°C)	Precursor	Reaction time (hrs)	Precursor concentration (%)
1	Distilled ethanol	25	MPTMS	2	2
2				8, 16, 24, 48	2
3				16	2, 4 and 6

In all the cases, for all the oxidized alloys, whatever the silane reagent, the samples were abundantly rinsed with fresh ethanol and then dried with pressurized argon.

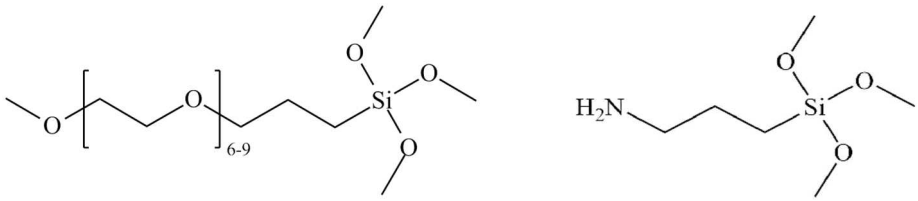

Scheme 1. Developed formula of MPTMS (left) and APTMS (right) silane reagents

2.5. Surface characterization

The microstructure of all the platelets, before and after oxidation or silanization, was checked by Scanning Electron Microscopy (SEM) using a Supra40 ZEISS FEG-SEM microscope operating at 5.0 kV.

The hydrophilicity of their surface was assessed by dynamic contact angle (CA) measurements. In detail, a drop of a calibrated volume (3 µL) is deposited on the surface of the investigated alloy. A camera follows the drop deposition and spreading. CA measurements are then achieved at the same time (5s) for all the samples on captured photos, using a DSA25 Krüss Advance drop shape Analyzer. These measurements are repeated 5 times on different areas of the surface sample and averaged to determine the final CA value, focusing only on the oxidized alloys.

To confirm siloxane grafting, FTIR spectroscopy was performed using a Thermo-Nicolet Nexus Model 8700 operating in attenuated total reflection (ATR) mode. Spectra were acquired in the range [500–4000 cm^{-1}] with a spectral resolution of 2 cm^{-1}.

Finally, their surface structure and chemical composition were determined by by Grazing Incidence X-ray diffraction (GIXRD) and X-ray photoelectron spectroscopy (XPS), respectively. GIXRD analysis was performed using a Panalytical Empyrean diffractometer, equipped with a parallel plate collimator, a multichannel detector (PIXcel 3D) and a Cu Kα X-ray source (1.5418 Å).The incidence angle ω is set at 0.5°, the angular range at 10°-80°. The step size is 0.04° and the time per step equal to 4 s.. Pattern processing (background estimation, peak search, and phase identification) were done thanks to the HighscorePlus

software (Panalytical ®). XPS spectra were recorded using a K-Alpha$^+$ system (ThermoFisher Scientific, East-Grinstead, UK) fitted with a micro-focused and monochromatic Al Kα X-ray source (1486.6 eV, spot size of 400 µm). The pass energy was set to 150 and 40 eV for the survey and the narrow high resolution regions, respectively. The spectra were calibrated against the (C—C/C—H) C 1s component set at 285 eV. The chemical composition was determined by using the manufacturer sensitivity factors using Avantage software, version 5.9902. Survey spectra to identify elements on the surface were collected in steps of 1 eV at pass energy of 150 eV. High-resolution ones of separate photoelectron lines (C, O, N, Si, Hf, Nb, Ta, Ti, and Zr) were taken by steps of 0.1 eV at pass energy of 40 eV. The photoelectron take-off angle was normal to the surface of the samples. The sample surface covered by the analysis is ($3.14\times0.4\times0.4 = 0.5024$ mm^2). Spectra processing (peak-fitting, area calculation…) was done with Avantage software.

2.6. Metal trace analysis in solution

In parallel, to the listed above material characterization techniques, X-ray Fluorescence spectroscopy (XRF) was performed on sterilized physiological solutions, typically PBS and Dulbecco's Modified Eagle cell culture Medium (DMEM), before and after one month contacting to the prepared alloys and their surface treated counterparts, to quantify any metal release. A trace methodology was applied inspired by previous works [45]. It consists in depositing 20 µL on a polycarbonate membrane, wait for the solvent to evaporate and repeat these steps 3 more times. A Panalytical Epsilon 3XL spectrometer, equipped with an Ag X-ray tube operating with 2 conditions : 50 kV during 300s for Hf, Nb, Ta and Zr, and 12 kV during 300s for Ti was used. Calibrations were established by preparing reference samples, with standard solutions of 1g/L (Inorganic Ventures) and using exactly the same membranes and measurement conditions. In the case of fine deposits, a linear relationship is obtained between the mass of the element and the intensity of the corresponding peak.

3. RESULTS AND DISCUSSION

The procedure applied in the present work includes two surface treatments: oxidation and silanization. For the oxidation, the effect of two main parameters was investigated: the surface roughness in relation to the alloy polishing grade and the chemical oxidation conditions in relation to the oxidation bath composition. For the silanization, a particular emphasis was made on the MPTMS reagent, varying its concentration and its reaction time.

3.1. Surface oxidation

In the remainder of this discussion, three kinds of samples were compared, one unpolished and two polished at 2000 and mirror grades, All of them were immersed in three different chemical oxidation baths, called respectively golden, grey and white conditions, in order to make a choice on the type of surface to be used for the silanization treatment. Also, the results of white oxidation will not be presented in this section, because this oxidation is too much corrosive leading to severe degradation of the surface, as already observed on conventional Ti alloys [46]. The formed oxide layer is porous and non-uniform in composition (see Figure SI-1 in the supporting information section).

GIXRD does not allow identifying any oxide phase at the surface of the treated alloys (see Figure SI-2). Only the peaks of the body-centered cubic alloy were identified. We attributed this feature to the very small thickness of the oxide layer (few nanometers), largely lower than the GIXRD analysis deepness (some hundreds of nanometers).

Reversely, XPS, which is a more surface sensitive analysis technique, confirmed the oxidation. All the high-resolution spectra recorded at the Hf 4f, Nb 3d, Ta 4f, Ti 2p, and Zr 3d XPS signals indicated that all these metallic elements exist at their +4 or +5 oxidation state on the alloys surface, as illustrated in Figure 1. Indeed, the measured binding energies for the

respective signals are almost equal to those usually reported for their monometallic oxides, namely HfO_2, Nb_2O_5, Ta_2O_5, TiO_2 and ZrO_2 (Table 2), suggesting that an unmixing occurred on the surface along with the oxidation.

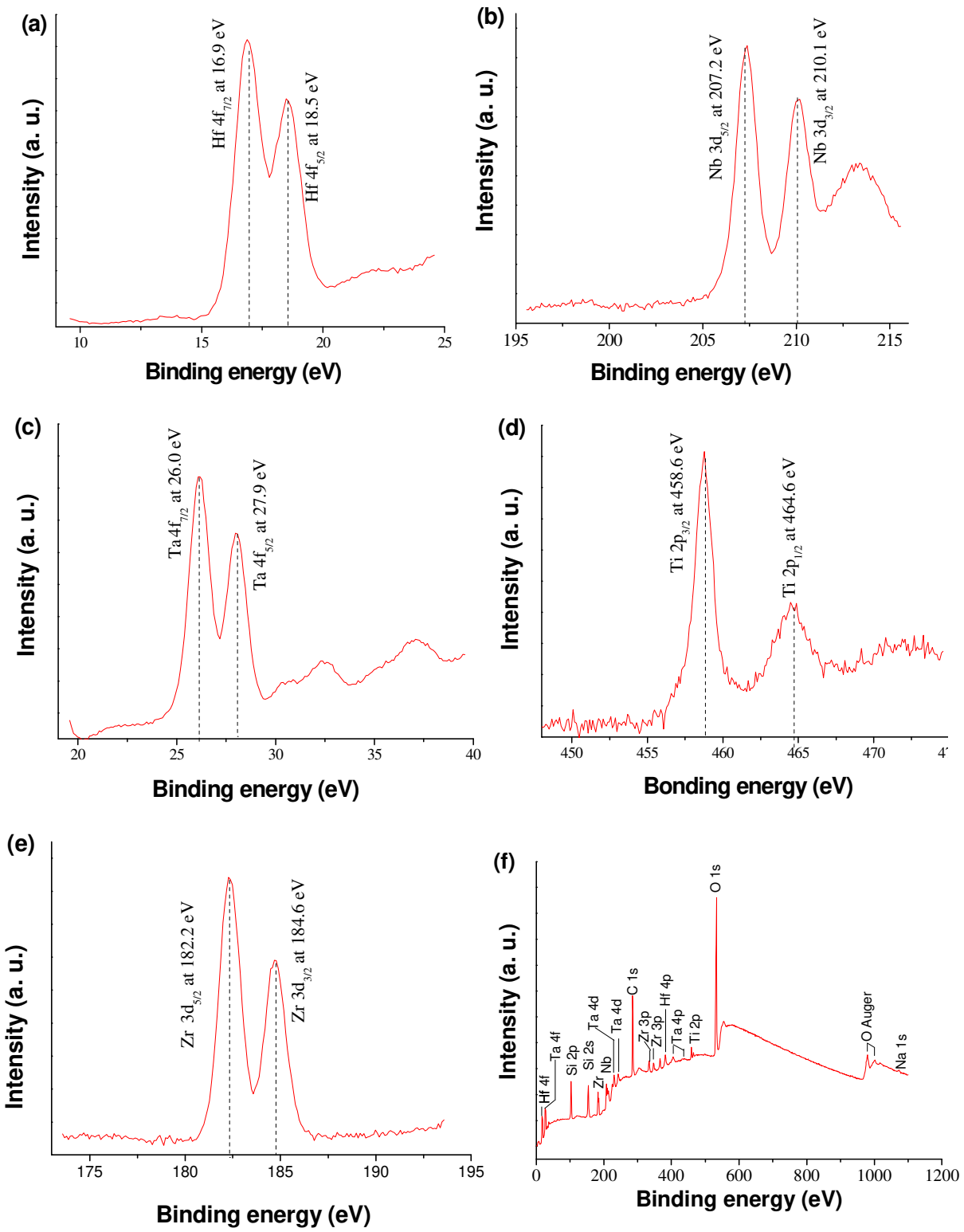

Figure 1: Hf 4f, Nb 3d, Ta 4f, Ti 2p, and Zr 3d, high-resolution XPS spectra (a, b, c, d, e, respectively) of HfNbTaTiZr alloy polished at miror grade and oxidized in water within golden conditions. The survey XPS spectrum is also given for information (e).

Usually, a non-negligible binding energy shift is observed in mixed metal oxides in comparison to the non-mixed ones [46-49]. This shift is due to the fact that, when two oxides were mixed to form a solid oxide solution, the cation of the more ionic metal oxide would become more ionic, and the cation of the more covalent metal oxide would become more covalent. Therefore, the charge of the more ionic cation, respectively the more covalent cation, is expected to be larger, respectively smaller, in the mixed oxide than in the pure oxides, making its core binding energy value larger, respectively smaller. To confirm such a behavior, we intentionally oxidized the unpolished HfNbTaTiZr alloy, and its polished counterparts, in air at 800°C. We obtained in all cases, a white powder. The XRD pattern of this powder matched very well with the superposition of the diffraction peaks of HfO_2, Nb_2O_5, Ta_2O_5, TiO_2 and ZrO_2 (Figure SI-3). The peaks are broadened, but their position is undoubtedly corresponding to the thermodynamically stable allotropes of these monometallic oxides.

Table 2: Binding energy (BE) values of the Hf 4f, Nb 3d, Ta 4f, Ti 2p and Zr 3d XPS signals for the HfNbTaTiZr alloy mirror polished and oxidized in water within golden conditions and in air at 800°C compared to those reported in the relevant literature for pure or doped HfO_2, Nb_2O_5, Ta_2O_5, TiO_2 and ZrO_2 oxide powders and/or films.

	BE(eV) Hf $4f_{7/2}$	**BE(eV) Nb $3d_{5/2}$**	**BE(eV) Ta $4f_{7/2}$**	**BE(eV) Ti $2p_{3/2}$**	**BE(eV) Zr $3d_{5/2}$**	**Ref**
HfNbTaTiZr oxidized in water	16.9	207.3	26.0	458.6	182.2	*This work*
HfNbTaTiZr oxidized in air	16.7	207.0	25.8	458.8	182.2	*This work*
Ta doped TiO_2	-	-	26.4	456.2	-	50
Nb doped TiO_2	-	206.7	-	456.2	-	50
Zr doped TiO_2	-	-	-	458.6	181.8	51
Pure TiO_2	-	-	-	458.5	-	50,52
Zr doped HfO_2	-	-	-	-	183.4	53,54
Pure HfO_2	16.7	-	-	-	-	55–57
Hf doped ZrO_2	-	-	-	-	181.7	56,58
Pure ZrO_2	-	-	-	-	182.4	59
Hf doped Ta_2O_5	17.1	-	26.2-26.3	-	-	60,61
Pure Ta_2O_5	-	-	26.7	-	-	62,63

Additionally, the recorded high-resolution Hf 4f, Nb 3d, Ta 4f, Ti 2p and Zr 3d XPS spectra of the white powder exhibited the same signatures than those previously observed on the

surface of water oxidized alloys (Table 2). Still, in the perspective of demonstrating that only monometallic oxides were formed, we were interested in comparing our XPS results with those of the literature dealing with the XPS signature of pure and mixed Hf, Nb, Ta, Ti and/or Zr powder and/or film oxides. Interestingly, Znad et al., who studied Ta and Nb-doped TiO_2 oxides [50], observed the expected cocktail effect with a shift in the binding energy of Ti 2p XPS signal from 458 in pure TiO_2 to 456 in Ta or Nb-doped one (Table 2). We did not observe these shifts on the Nb 3d, Ta 4f, and Ti 2p signals of our oxidized alloys. Armeleo et al. [57] and Lu et al. [60,61] also observed this cocktail effect by comparing the Hf 4f signal in pure HfO_2 and Zr doped HfO_2 and the signal of Ta 4f in pure TaO_2 and Hf doped TaO_2 oxide, respectively. And, once again, we did not observe such shifts on the Hf 4f, Ta 4f and Zr3d signals of our oxidized alloys. So, monometallic oxides were formed at the surface of all our treated alloys despite their initial alloying as a single metallic solid solution phase.

Now, comparing the surface chemical composition of our samples, differences appeared from one sample to another, depending much more on the oxidation conditions than on the polishing ones (Table 3). Indeed, the samples oxidized in the solution of oxalic acid with hydrogen peroxide (grey conditions) are strongly lixiviated, whatever their polishing grade, with a net loss of Nb, Ta, and Ti elements. In the case of the samples oxidized in the solution of oxalic acid without hydrogen peroxide (golden conditions), the Hf, Nb, Ta, Ti and Zr contents remained equivalent, meaning that the surface of the alloys is still equimolar.

Table 3: Surface atomic composition of the HfNbTaTiZr alloy polished at different grades and oxidized in water within grey and golden conditions, compared to that of the same polished alloys and heated in air at 800°C.

Oxidation type	Sample	%Hf	%Nb	%Ta	%Ti	%Zr
Aqueous grey oxidation	Unpolished	23,0	14,0	18,0	12,0	33,1
	Polished 2000	23,1	14,0	14,9	14,1	34,0
	Polished mirror	22,3	13,5	17,0	12,0	36,0
Aqueous golden oxidation	Polished 2000	21,0	19,0	22,0	18,0	20,0
	Polished mirror	22,1	19,0	21,1	17,1	21,0

Finally, in the case of the unpolished samples, because of a probable thick carbon contamination deposits on their surface, we have very weak metallic concentrations, not at all representative of the bulk composition of the bar alloy, particularly for those treated within soft oxidation conditions. The carbon deposit has not been digested, masking, therefore, the inorganic surface of the unpolished alloys during XPS analysis. As a consequence, we decided to mainly focus on the polished samples, and particularly those oxidized in water within golden conditions for the desired applications. In order to tentatively make a final choice between the two grades of polishing, 2000 and mirror, we performed surface morphology analyses of their surface using both SEM top view observations and water contact angle measurements. The comparison of the recorded SEM micrographs on the polished alloy at 2000 and mirror grades and subsequently oxidized in water within golden conditions showed some morphological differences (Figure 2). The sample polished at 2000 grade exhibits a denser surface than that polished at mirror grade. Moreover, the latter sample exhibits also a submicrometer-sized surface porosity, which is also evidenced by the contact angle measurements. Indeed, whereas the former sample evidences a surface wettability and then a hydrophilicity increase upon oxidation, with a net decrease of the average contact angle from about 60° to about 5° after aqueous treatment, the later does not. The spread water droplets infiltrate its oxide layer, making the measurement impossible (Figure 3). The sample polished at 2000 grade and oxidized within the golden oxidation was thus retained for the silanization step.

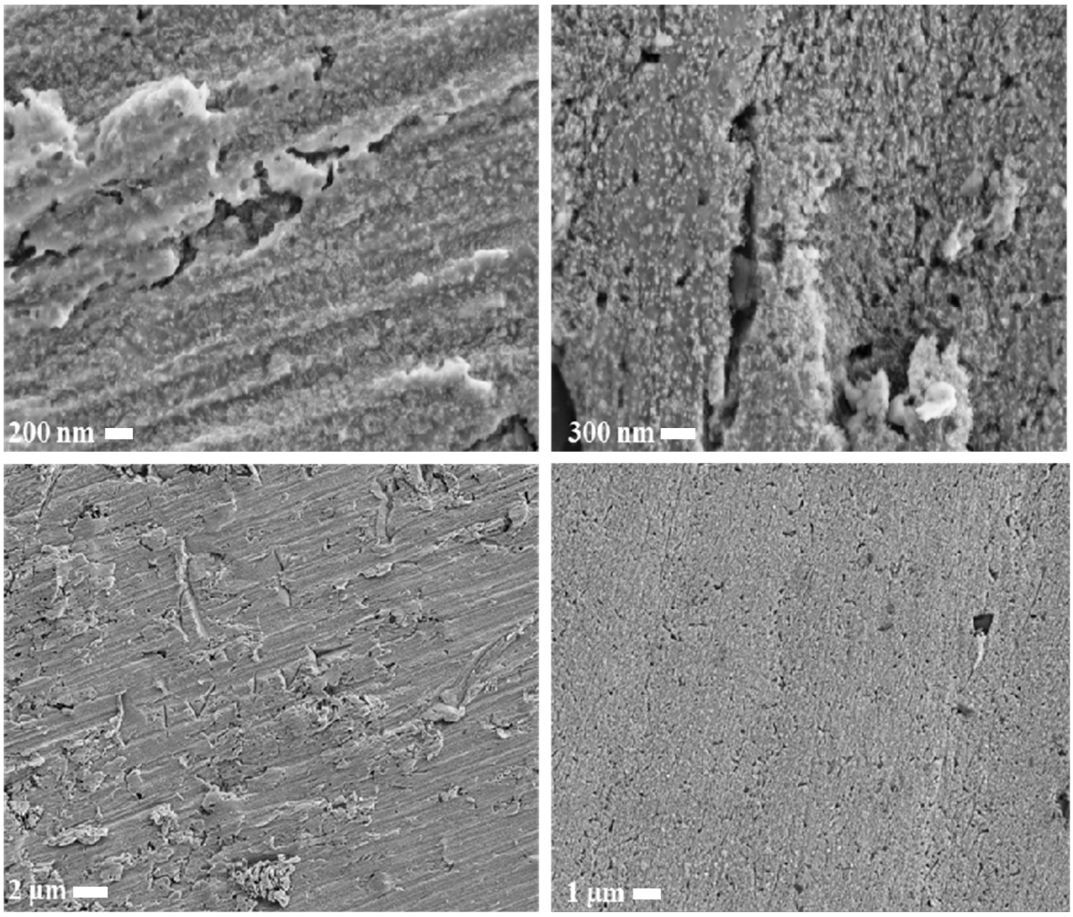

Figure 2: Surface SEM images of the alloys polished at 2000 (left) and mirror (right) grades and oxidized within golden conditions.

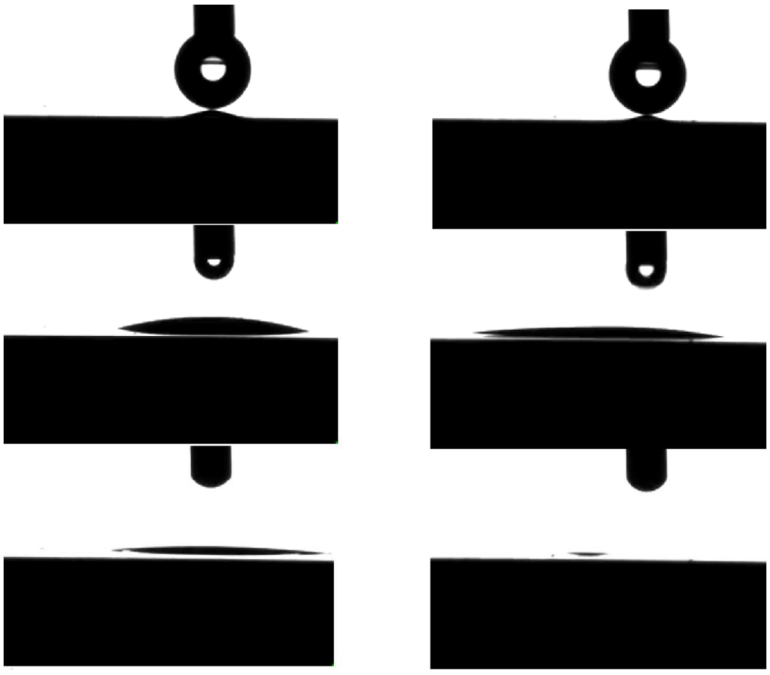

Figure 3: Contact angle measurement of the alloys polished at 2000 (left) and mirror (right) grades and oxidized within golden conditions.

3.2-Surface silanization

Preliminary APTMS grafting experiments allowed us to fix the ability of our polished at grade 2000 and oxidized under golden conditions HfNbTaTiZr alloy to be silanized. Within the explored operating conditions, namely a nominal APTMS concentration of 2 % and a reaction time as short as 2 hrs, we succeeded to grow a dense and thick coverage for a (see Figure SI-4 and Figure SI-5). As expected these conditions are found to be far from the required ones for MTMPS attachment. All the MPTMS FTIR signatures are missing in the recorded spectra on the samples treated with MPTMS within the same operating conditions than those used for APTMS (Figure 4). Whereas the FTIR spectrum of free MPTMS spectrum (Figure 4a) evidenced bands characteristic of the CH_3 rocking [62], Si–O (in Si–O–CH_2) stretching [63,64], Si–O stretching [63,64], Si-O–CH_2 bending [64], CH_2 rocking [64,65] and H–C–H (in CH_2) bending [62] at 835, 953, 1090 cm^{-1}, 1241, 1176 and 1391 cm^{-1}, respectively, that of grafted alloys did not (Figure 4a). Also, the bands at 2980 and 2875 cm^{-1}, commonly assigned to the symmetric and asymmetric C–H (in CH_3) stretching [64] vibrations are missing (Figure 4a). Reversely, by increasing the reaction time and also the MPTMS nominal concentration (Table 1), we significantly improved the grafting conditions. All the characteristics MPTMS bands were identified in the spectra of the alloys contacted with MPTMS for 16 hrs and more (Figure 4b), with an intensity which increases when the reaction time and/or the precursor concentration increases. This is typically the case of the bands centered at 1090 cm^{-1} (Si–O vibration) and 2980 cm^{-1} (C–H vibration) as illustrated in Figure 4b and Figure 4c. Note that the highest intensities for these bands were obtained for the sample treated for 48 hrs, fixing the nominal MPTMS concentration to 2%. For this sample, the band attributed to the Si–O–CH_2 bending vibrations at 1241 cm^{-1} disappears completely (Figure 4b), meaning that, within these reaction conditions, each MTMS molecule loses its 3 methoxy groups, after their nucleophilic substitution within the silicon coordination sphere by 3 hydroxyl groups from the alloy surface.

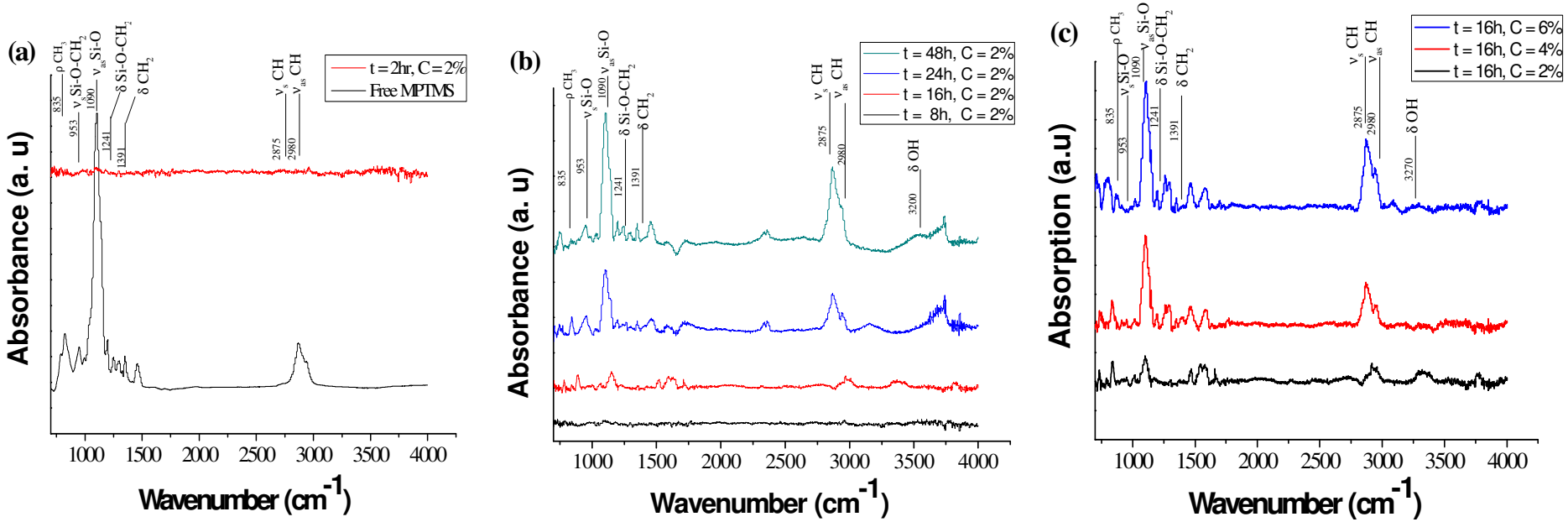

Figure 4: Comparison of the ATR-FTIR spectra recorded on free MPTMS and the treated alloy for a reaction time of 2 hrs, fixing the nominal MPTMS concentration to 2 % (a). Comparison of the ATR-FTIR spectra recorded on the treated alloys for different silanization reaction time, fixing the nominal MPTMS concentration again to 2 % (b). Comparison of the ATR-FTIR spectra recorded on the treated for different MTMPS nominal concentrations, fixing the reaction time to 16 hrs (c).

This reactivity leads to the attachment of each engaged Si atom to the metal surface through three covalent metal-O-Si bonds, achieving a strong attachment of the MPTMS organic layer to the alloy surface. This must be underlined because it is crucial, for the desired application, that the organic coating remains anchored to the implant surface, whatever its chemical and mechanical environment.

XPS analysis was also performed on the silanized samples to confirm the ATR-FTIR results. The atomic concentrations of the different surface elements are summarized hereafter in Table 4, focusing on the two samples series, that corresponding to the variation of the reaction time from 16 to 48 hrs, fixing the nominal MPTMS concentration at 2%, and that corresponding to the variation of the nominal MPTMS concentration from 2 to 6 %, fixing the reaction time to 16 hrs.

Table 4: Surface atomic composition of the HfNbTaTiZr alloy polished at grade 2000, oxidized in water within golden conditions and reacted to MTPMS molecules in ethanol for different times and/or nominal siloxane concentrations.

MPTMS nominal concentration (%)	**Reaction time (hrs)**	Surface chemical composition (at.-%)							
		C	**O**	**Si**	**Hf**	**Nb**	**Ta**	**Ti**	**Zr**
0	**0**	28.2(*)	56.1(*)	3.0(*)	2.6(*)	2.7(*)	2.6(*)	2.5(*)	2.5(*)
2	**16**	32.4	47.0	7.5(**)	2.6	2.7	2.7	2.5	2.5
2	**24**	60,0	27.4	11.7(**)	0,2	0,2	0,2	0,2	0,2
2	**48**	71,0	26.5	2.4(**)	-(***)	-(***)	-(***)	-(***)	-(***)
4	**16**	41.6	40.5	6.8	2.2	2.3	2.2	2.2	2.2
6	**16**	46.3	40.1	6.0	1.5	1.5	1.5	1.5	1.5

(*) Data inferred from the XPS spectrum recorded on the oxidized alloy just before its silanisation

(**) Silicon content does not vary monotonically in this sample series, due to random silica contamination occasioned during the polishing process. For this reason, this element has not used a fingerprint of the MPTMS grafting, and only the carbon and oxygen content increase was used for such a purpose.

(***) For these reaction conditions, XPS analysis does not allow identifying the presence of any metallic elements meaning that the thickness of the formed organic layer on the sample surface is larger than the depth analyzed by XPS (less than 10 nanometers).

First of all, by comparing the high resolution XPS Si 2p signal from one sample to another for these two series, and from any of them to that of the non-silanized sample, one may note that

the intensity of this signal is never zero, and it is higher in the silanized samples than in the non-silanized one. Also, the intensity of this signal does not vary monotonically as the reaction time or the precursor concentration increases (Figure SI-6). It can be thus concluded that the appearance of the Si 2p XPS peak at about 103 eV can not be used as a silanization fingerprint. Random Silicon contamination related to the polishing step (the use of silica colloids and/or silicon carbide discs) exist in all the samples and does not allow direct quantification of the grafting process.

Second, by comparing the high-resolution XPS C 1s signal at around 285 eV from one sample to another for these two series, and from any of them to that of the non-silanized sample, one may note that the amount of carbon on the surface of the oxidized alloy increases when the reaction time and/or the silane nominal concentration increase, meaning an increase in the amount of attached MPTMS molecules (Figure 5). To be more precise, this peak is, in fact, a double peak, centered at 285 and 286 eV, and related to C-C/C-H and C-O-C species, respectively (see the peak-fitting plots in Figure SI-7) [66-68]. Interestingly, the intensity of the ether contribution, which is specific to the MPTMS molecules (see scheme 1), increases when the reaction time and/or the silane concentration increases, confirming undoubtedly the grafting.

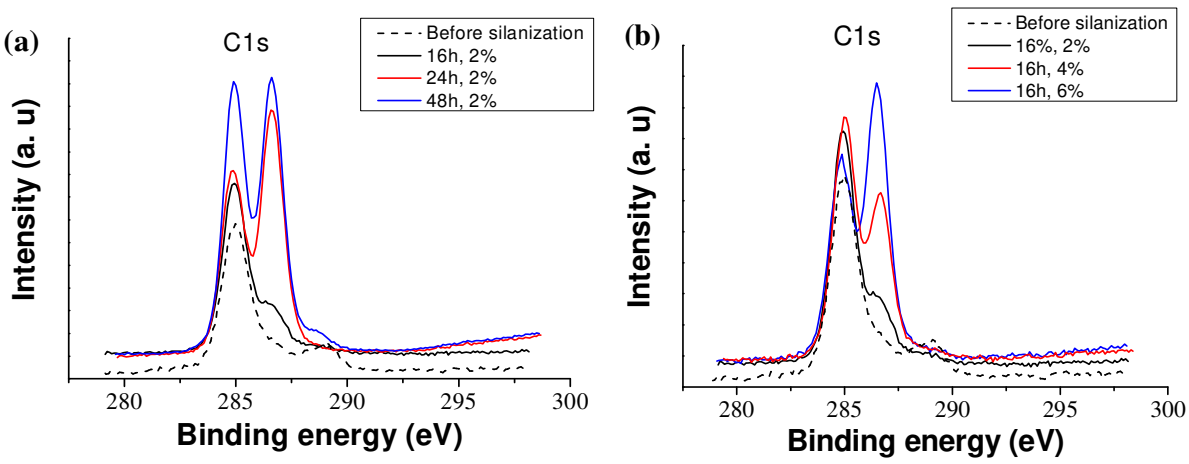

Figure 5: High resolution C 1s XPS spectrum of HfNbTaTiZr alloy polished at grade 2000 and oxidized in water within golden conditions compared to those of the same sample after its

reaction with MTPMS (2%) for 16, 24 and 48 hrs (a), or for 16 hrs with a MPTMS nominal concentration of 2 , 4 and 6% (b). For the two set of samples, the C 1s XPS signature before grafting is given for comparison (see dashed black line).

The same comparison performed around the XPS O 1s signal also gives similar information. It shows that this signal is, in fact, the convolution of two contributions, an organic one, at 532.0 eV, inferred from the ether groups of the attached MPTPS molecules on the surface of the treated alloys, and an inorganic one, at 531.0 eV, originated from the involved oxide lattices (Figure 7). Interestingly, the later contribution decreases drastically to disappear for the sample corresponding to a reaction time of 48 hrs, suggesting a total and dense alloy coating. Beside this peak intensity change, a slight peak position shift proceeds (see Figure SI-8 in the supporting information section). This feature is also correlated to a progressive coverage of the metal oxide surface, through Si-O-Metal covalent bonding. So even if one of the Hf-O-Si, Nb-O-Si, Ta-O-Si, Ti-O-Si or Zr-O-Si bonds are created selectively at the beginning of the silanization reaction, it is very likely that after 48 hrs, this selectivity is averaged and all these bonds become effective.

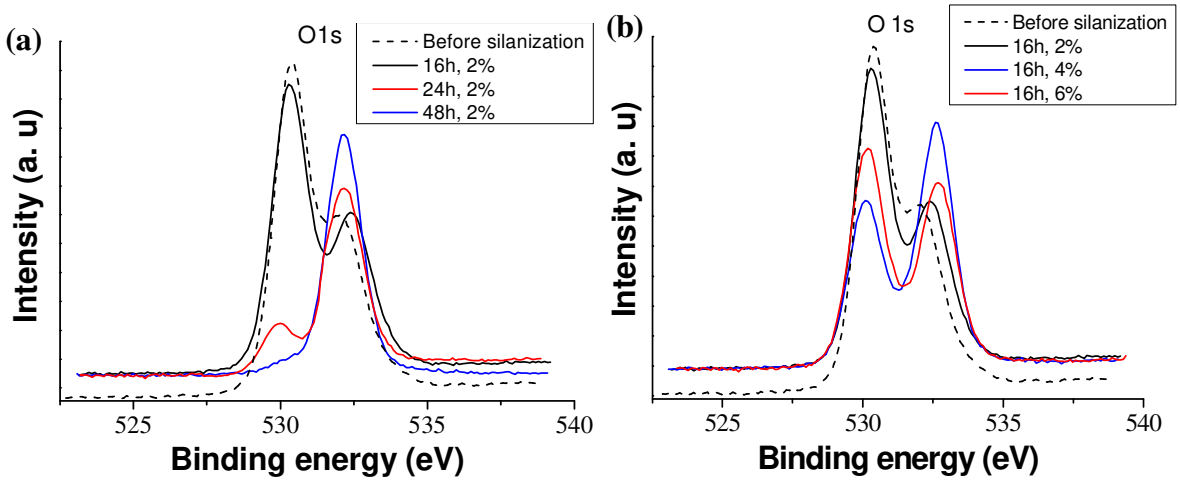

Figure 6: High resolution O 1s XPS spectrum of HfNbTaTiZr alloy polished at grade 2000 and oxidized in water within golden conditions compared to those of the same sample after its reaction with MTPMS (2%) for 16, 24 and 48 hrs (a), or for 16 hrs with a MPTMS nominal concentration of 2, 4 and 6% (b). For the two set of samples, the O 1s XPS signature before grafting is given for comparison

This is confirmed by the disappearance, for this sample, of the Hf, Nb, Ta, Ti and Zr XPS signatures, in its survey spectrum and its respective Hf 4f, Nb 3d, Ta 4f, Ti 2p and Zr3d high-resolution XPS spectra (Figure 7).

So, for these silanization reaction conditions, a continuous organic layer was successfully deposited on the oxidized alloy. This layer is assumed to be of about 10 nm in thickness. Indeed, focusing in the whole survey XPS spectra shape, one may observe that background becomes flatter when the grafting reaction time increases suggesting a thickening of the grafted layers. In the same time, for the sample corresponding to the longest reaction time (blue line in Figure 7f), the survey spectrum does not have a completely flat horizontal background. This means that though the PEGylated silane layer is there, it does not completely screen the inelastically emitted core electrons from the underlying alloy. Such feature is often reported when the grafted layered shell is not thick enough to completely screen the underlying substrate [69,70]. This is typically the case when the thickness of the coating does not exceed the analysis depth, *i.e.* 10 nm.

So, on these bases, we decided to pursue our investigations on this sample precisely, in order to test the efficiency of the coating toward eventual chemical attack, when immersed for a long time in biomimetic aqueous environments.

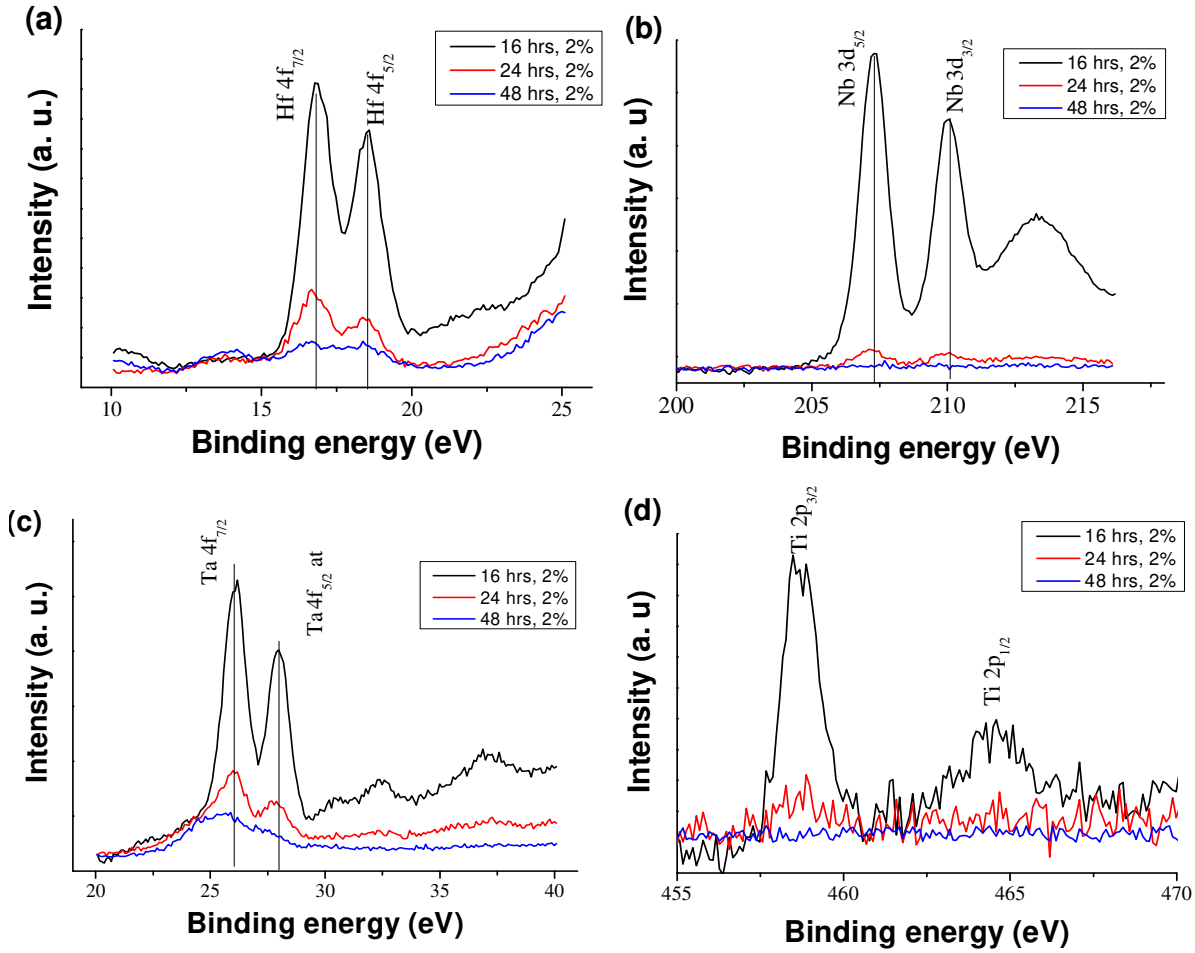
(a)
Intensity (a. u.)
Hf 4f7/2
Hf 4f5/2
16 hrs, 2%
24 hrs, 2%
48 hrs, 2%
10
15
20
25
Binding energy (eV)
(b)
Intensity (a. u)
Nb 3d5/2
Nb 3d3/2
16 hrs, 2%
24 hrs, 2%
48 hrs, 2%
200
205
210
215
Binding energy (eV)
(c)
Intensity (a. u.)
Ta 4f7/2
Ta 4f5/2 at
16 hrs, 2%
24 hrs, 2%
48 hrs, 2%
20
25
30
35
40
Binding energy (eV)
(d)
Intensity (a. u)
Ti 2p3/2
Ti 2p1/2
16 hrs, 2%
24 hrs, 2%
48 hrs, 2%
455
460
465
470
Binding energy (eV)

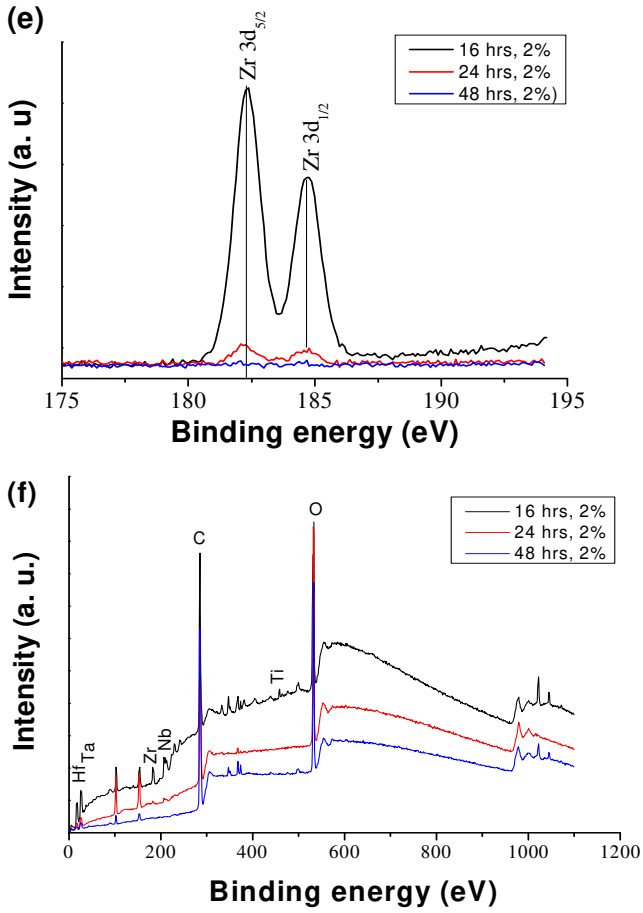

Figure 7: High-resolution Hf 4f, Nb 3d, Ta 4f, Ti 2p and Zr 3d XPS spectra (a, b, c, d and e, respectively) of HfNbTaTiZr alloy polished at grade 2000, oxidized in water within golden conditions and then reacted to MTPMS fixing the nominal siloxane concentration to 2% and varying the reaction time from 16 to 48 hrs. The survey spectra of all the analyzed samples are also given for information (c).

3.3. Immersion in a physiological medium

As a preliminary biological assay, focusing on the alloy polished at 2000 grade, its oxidized within golden conditions (without H_2O_2) counterpart and that coated by MPTMS within optimized silanization conditions (a reaction time of 48 hrs for a nominal silane concentration of 2%), two different solutions, a PBS buffer (M1) and a DMEM standard nutrient mixture for cell culture (M2), were selected to test the chemical stability of the samples. In practice, the solutions were filtered (0.2 µm) and stored in a sterilized glass vessel (autoclaved at 120°C) within a laminar flow hood, to avoid any bacteriological contamination, before use. Also, still operating in a laminar flow hood, the selected platelet was exposed to UV (365 nm) for a

couple of minutes and then immersed in the selected solutions for one month (30 days) in closed sterilized and light-opaque glass bottles. At the end of the experiment, the supernatants were analyzed by XRF while the platelets were analyzed by XPS.

XRF was carried out to detect possible traces of released metals, but after four successive 20 µL deposits drawn in each physiological medium (M1 and M2), no traces of Hf, Nb, Ta Ti nor Zr metals were evidenced. The same results were obtained, whatever the analyzed supernatants, those in which untreated alloys were immersed and those in which treated alloys were immersed. Of course, these results must be considered with cautions, since they are restricted by XRF detection limits. As a reminder, the detection limits of Hf, Nb, Ta, Ti, and Zr, within our operating conditions, are of 54, 49, 63, 30 and 42 ng, corresponding to minimal concentrations of 675, 612, 787, 375, 525 µg/L, respectively.

Once removed from the physiological environment, the platelets were abundantly rinsed with ethanol under sonication and dried under argon flow before XPS analysis. The obtained results are more contrasted than those inferred from XRF ones. Indeed, whereas, bare and oxidized alloy exhibit slight Nb and Ti losses, with a decrease of their respective atomic content by comparison with the fresh samples, their silanized counterpart does not (Table 5). After MPTMS grafting, the density and the thickness of the formed organic layer make the HEA metallic elements completely buried under it, escaping from any PBS or DMEM corrosion effect. The organic coating appeared to be still present slightly affected by the prolonged immersion in the selected biomimetic solutions, particularly DMEM one, since a slight increase of the nitrogen content was observed (Table 5) due to probable amino acids adsorption.

Table 5: Surface atomic composition of the HfNbTaTiZr alloy polished at grade 2000 (bare alloy), oxidized in water within golden conditions (oxidized) and reacted to MPTMS (2%) for 48 hrs after their immersion for one month in M2 media.

Medium	Sample	Surface chemical composition (at.-%)

		C	O	N	Si	Hf	Nb	Ta	Ti	Zr
M1	bare	43.8	42.3	1.3	0.7	2.6	**2.0**	2.6	**2.0**	2.7
	oxidized	47.1	40.9	1.2	1.0	2.1	**1.8**	2.1	**1.8**	2.1
	silanized	69.6	28.1	1.5	0.9	-(*)	-(*)	-(*)	-(*)	-(*)
M2	bare	55.17	29.83	6.12	2.80	1.4	**1.0**	1.4	**1.0**	1.4
	oxidized	53.09	29.31	7.92	3.20	1.5	**1.0**	1.5	**1.0**	1.4
	silanized	68.27	20.18	11.05	0.50	-(*)	-(**)	-(**)	-(**)	-(**)

(**) XPS analysis does not allow identifying the presence of any metallic elements meaning that the thickness of the formed organic layer on the sample surface is larger than the depth analyzed by XPS (less than 20 nanometers).

CONCLUSION

In the present work, we have compared different reactions conditions for functionalization of HfNbTaTiZr equimolar for materials bio-implant applications. Qualitatively, the oxidation step leads to unmixed monometallic oxide layer: TiO_2, Nb_2O_3, ZrO_2, Hf_2O_3, and Ta_2O_5 whatever the polishing grade and the oxidation conditions (golden or grey). Quantitatively, the sample polished 2000 oxidized golden (without H_2O_2) retains the best surface chemical stoichiometry. The appearance of Si-O and C-H bonds at 1100 and 2900 cm^{-1} during the ATR-FTIR analysis of oxidized and functionalized alloys confirms the grafting of MPTMS molecules to the surface. The MPTMS concentration in the pure ethanol and the reaction time has a direct influence on the quality of the grafted layer on the surface of HfNbTaTiZr. Interestingly, combining XRF and XPS analyses, we demonstrated that this coating prevents the chemical surface alteration of the alloy when contacted, for a long time (one month), to biomimetic media, like PBS and DMEM, promoting the use of surface silanized equimolar HfNbTaTiZr as bio-implant material definitively.

ACKNOWLEDGMENTS

The French ANR (*Agence Nationale de la Recherche*) and CGI (*Commissariat à Investissement d'Avenir*) are gratefully acknowledged for their financial support of this work through the Labex SEAM grant (N°ANR 11 LBX 086 and ANR 11 IDEX 05 02). The authors

acknowledge the access to the XPS platform of ITODYS lab. (Paris Diderot University) that is supported by the *Ile-de-France* Regional Counsil trough the SESAME grant (N°16016303). Finally, they want also to thank Mrs. Ivonne Cocca (Paris Diderot University) for her technical assistance during XRF measurements°.

REFERENCES

1 M. Long and H. J. Rack, Titanium alloys in total joint replacement—a materials science perspective, *Biomaterials*, 1998, **19**, 1621–1639.

2 S. J. L. Sullivan and L. D. T. Topoleski, Surface Modifications for Improved Wear Performance in Artificial Joints: A Review, *JOM*, 2015, **67**, 2502–2517.

3 P. Uhlenberg, *International Handbook of Population Aging*, Springer Science & Business Media, 2009.

4 M. Geetha, A. K. Singh, R. Asokamani and A. K. Gogia, Microstructure and properties of a refractory $NbCrMo_{0.5}Ta_{0.5}TiZr$ alloy, *Prog. Mater. Sci.*, 2009, **54**, 397–425.

5 J. L. Katz, Anisotropy of Young's modulus of bone, *Nature*, 1980, **283**, 106–107.

6 W. Murphy, J. Black and G. Hastings, Eds., *Handbook of Biomaterial Properties*, Springer-Verlag, New York, 2nd edn., 2016.

7 A. Djemai and J.-J. Fouchet, Process for producing a beta-alloy Titanium Niobium Zirconium (TNZ) with a very low modulus of elasticity for biomedical applications and its embodiment by additive manufacturing, *United States Patent Application n°20190111482* April 2019

8 K. T. Kim, M. Y. Eo, T. T. Hoang Nguyen and S. M. Kim, General review of titanium toxicity, *Int. J. Implant Dent.* 2019, **5**, 10.

9 D. R. Haynes, S. D. Rogers, S. Hay, M. J. Pearcy and D. W. Howie, The differences in toxicity and release of bone-resorbing mediators induced by titanium and cobalt-chromium-alloy wear particles, *J. Bone Joint Surg. Am.* 1993, **75**, 825–839.

10 M. Geetha, A. K. Singh, R. Asokamani, A. K. Gogia, Ti based biomaterials, the ultimate choice for orthopaedic implants – A review, *Prog. Mater. Sci.* 2009 **54**, 397–425.

11 B. M. Isaacson and S. Jeyapalina, Osseointegration: a review of the fundamentals for assuring cementless skeletal fixation, Orthopedic Res. Rev. 2014, **6**, 55-65.

12 M. Saini, Y. Singh, P. Arora, V. Arora, K. Jain, Implant biomaterials: A comprehensive review, World J. Clin. Cases 2015, **3**, 52–57.

13 D. R. Sumner, T. M. Turnera, R. Igloria, R. M. Urbana, J. O. Galante, Functional adaptation and ingrowth of bone vary as a function of hip implant stiffness, *J. Biomechanics*1998, **31**, 909–917.

14 O. N. Senkov and C. F. Woodward, Microstructure and properties of a refractory NbCrMo0.5Ta0.5TiZr alloy, *Mater. Sci. Eng. A* 2011, **529**, 311–320.

15 J.-P. Couzinié, O. N. Senkov, D. B. Miracle and G. Dirras, Comprehensive data compilation on the mechanical properties of refractory high-entropy alloys, *Data Brief* 2018, **21**, 1622–1641.

16 Y. Okazaki, A New Ti–15Zr–4Nb–4Ta alloy for medical applications, *Curr. Opin. Solid State Mater. Sci.* 2001, **5**, 45–53.

17 T. Nagase, Y. Iijima, A. Matsugaki, K. Ameyama and T. Nakano, Design and fabrication of Ti–Zr-Hf-Cr-Mo and Ti–Zr-Hf-Co-Cr-Mo high-entropy alloys as metallic biomaterials, *Mater. Sci. Eng.: C* 2020, **107**, 110322.

18 T. Hori, M. Todai, T. Nakano, T. Nagase and A. Matsugaki, Development of non-equiatomic Ti-Nb-Ta-Zr-Mo high-entropy alloys for metallic biomaterials, S*cripta Mater* 2019,**172**, 83–87.

19 V. Braic, M. Balaceanu, M. Braic, A. Vladescu, S. Panseri and A. Russo, Characterization of multi-principal-element (TiZrNbHfTa)N and (TiZrNbHfTa)C coatings for biomedical applications, *J. Mech. Behav. Biomed. Mater.*, 2012, **10**, 197–205.

20 G. Abadias, L. E. Koutsokeras, A. Siozios, P. Patsalas, Stress, phase stability and oxidation resistance of ternary Ti–Me–N (Me=Zr, Ta) hard coatings, *Thin Solid Films*, 2013, **538**, 56–70.

21 A. Escudeiro, T. Polcar, A. Cavaleiro, a-C(:H) & a-C(:H)_Zr coatings deposited on biomedical Ti-based substrates: Tribological properties, *Thin Solid Films*, 2013, **538**, 89–96.

22 C.-M. Cotrut, V. Braic, M. Balaceanu, I. Titorencu, M. Braic, A. C. Parau. Corrosion resistance, mechanical properties and biocompatibility of Hf-containing ZrCN coatings, *Thin Solid Films*, 2013, **538**, 48–55.

23 A. Shah, S. Izman, S. N. F. Ismail, H. Mas Ayu, C. G. Che Kob, R. Daud and M. R. Abdul Kadir, The Influence of Ultrasonic Vibration Frequency on the Properties of TiN Coated Biomedical Ti–13Zr–13Nb, *Metals*, 2018, **8**, 317.

24 M. Szklarska, G. Dercz, W. Simka and B. Łosiewicz, AC impedance study on the interfacial properties of passivated $Ti_{13}Zr_{13}Nb$ alloy in physiological saline solution, *Surf. Interface Anal.* 2014, **46**, 698–701.

25 D.-B. Zhou, S.-G. Wang, S.-P. Wang, H.-J. Ai and J. Xu, MRI compatibility of several early transition metal based alloys and its influencing factors, *J. Biomed. Mater. Res. B Appl. Biomater.* 2018, **106**, 377–385.

26 S.-P. Wang and J. Xu, TiZrNbTaMo high-entropy alloy designed for orthopedic implants: As-cast microstructure and mechanical properties, *Mater. Sci. Eng. C* 2017, **73**, 80–89.

27 M. Todai, T. Nagase, T. Hori, A. Matsugaki, A. Sekita and T. Nakano, Novel TiNbTaZrMo high-entropy alloys for metallic biomaterials, *Scr. Mater.* 2017, **129**, 65–68.

28 G. Dirras, L. Lilensten, P. Djemia, M. Laurent-Brocq, D. Tingaud, J.-P. Couzinié, L. Perrière, T. Chauveau and I. Guillot, Elastic and plastic properties of as-cast equimolar TiHfZrTaNb high-entropy alloy, *Mater. Sci. Eng. A* 2016, **654**, 30–38.

29 L. Lilensten, J.-P. Couzinié, L. Perrière, A. Hocini, C. Keller, G. Dirras and I. Guillot, Study of a bcc multi-principal element alloy: Tensile and simple shear properties and underlying deformation mechanisms, *Acta Mater* **142** (2018) 131–141.

30 G. Dirras, J. Gubicza, A. Heczel, L. Lilensten, J.-P. Couzinié, L. Perrière, I. Guillot and A. Hocini, Microstructural investigation of plastically deformed $Ti_{20}Zr_{20}Hf_{20}Nb_{20}Ta_{20}$ high entropy alloy by X-ray diffraction and transmission electron microscopy, *Mater. Charact.* 2015, **108**, 1–7.

31 B. Guennec, V. Kentheswaran, L. Perrière, A. Ueno, I. Guillot, J.-Ph. Couzinié and G. Dirras, Four-point bending fatigue behavior of an equimolar BCC HfNbTaTiZr high-entropy alloy: Macroscopic and microscopic viewpoints, *Materialia* 2018, **4**, 348–360.

32 M. Niinomi, M. Nakai and J. Hieda, Development of new metallic alloys for biomedical applications, *Acta Biomater.* 2012, **8**, 3888–3903.

33 Y. Y. Zhao, Z. F. Lei, Z. P. Lu, J. C. Huang and T. G. Nieh, A simplified model connecting lattice distortion with friction stress of Nb-based equiatomic high-entropy alloys, *Mater. Res. Lett.* 2019, **7**, 340–346.

34 J. Zýka, J. Málek, J. Veselý, F. Lukáč, J. Čížek, J. Kuriplach and O. Melikhova, Microstructure and Room Temperature Mechanical Properties of Different 3 and 4 Element Medium Entropy Alloys from HfNbTaTiZr System, *Entropy* 2019, **21**, 114.

35 M. Niinomi, Recent research and development in titanium alloys for biomedical applications and healthcare goods, *Sci. Technol. Adv. Mater.* 2003, **4**, 445–454.

36 P. Dubruel, E. Vanderleyden, M. Bergadà, I. De Paepe, H. Chen, S. Kuypers, J. Luyten, J. Schrooten, L. Van Hoorebeke and E. Schacht, Comparative study of silanisation reactions for the biofunctionalisation of Ti-surfaces, *Surf. Sci.* 2006, **600**, 2562–2571.

37 A. Pier-Francesco, R. J. Adams, M. G. J. Waters and D. W. Williams, Titanium surface modification and its effect on the adherence of Porphyromonas gingivalis: an in vitro study, *Clin. Oral Implants Res.* 2006, **17**, 633–637.

38 S. Izman, M. R. Abdul-Kadir, M. Anwar, E. M. Nazim, R. Rosliza, A. Shah and M. A. Hassan, "Surface Modification Techniques for Biomedical Grade of Titanium Alloys: Oxidation, Carburization and Ion Implantation Processes" in *Titanium Alloys - Towards Achieving Enhanced Properties for Diversified Applications,* Edited by A.K.M. Nurul Amin, IntechOpen (1st Edition), 2012, 202–228.

39 A. Rodríguez-Cano, P. Cintas, M.-C. Fernández-Calderón, M.-Á. Pacha-Olivenza, L. Crespo, L. Saldaña, N. Vilaboa, M.-L. González-Martín and R. Babiano, Controlled silanization–amination reactions on the Ti6Al4V surface for biomedical applications, *Colloids Surf. B Biointerfaces*, 2013, **106**, 248–257.

40 J.-P. Couzinié, G. Dirras, L. Perrière, T. Chauveau, E. Leroy, Y. Champion and I. Guillot, Microstructure of a near-equimolar refractory high-entropy alloy, *Mater. Lett.*, 2014, **126**, 285–287.

41 Y. Gigi, S. Bayram, C. J. Ablenas, A. Szuchmacher Blum and G. Cosa, Efficient One-Step PEG-Silane Passivation of Glass Surfaces for Single-Molecule Fluorescence Studies *ACS Appl. Mater. Interfaces* 2018, **10**, 39505–39511.

42 S. Jo, K. Park, Surface modification using silanated poly(ethylene glycol)s, *Biomaterials*, 2000, **21**, 605-616.

43 R.-V. Ostaci, D. Damiron, S. Al Akhrass, Y. Grohens and E. Drockenmuller, Poly(ethylene glycol) brushes grafted to silicon substrates by click chemistry: influence of PEG chain length, concentration in the grafting solution and reaction time, *Polym. Chem.* 2011, **2**, 348-354

44 W.E. Rapp and E. Bayer, Dynamics and application of polystyrene immobilized PEG chains, *Proc. ACS Div. Polym. Mater. Sci. Eng.* 1993, **69**, 521.

45 E. Marguí, M. Hidalgo and I. Queralt, XRF spectrometry for trace element analysis of vegetation samples, *Spectrosc. Eur.*, 2007, **19**, 13–17.

46 S. Chaguetmi, S. Achour, L. Mouton, P. Decorse, S. Nowak, C. Costentin, F. Mammeri and S. Ammar, TiO_2 nanofibers supported on Ti sheets prepared by hydrothermal corrosion: effect of the microstructure on their photochemical and photoelectrochemical properties, *RSC Adv.*, 2015, **5**, 95038–95046.

47 T. L. Barr, Recent advances in x-ray photoelectron spectroscopy studies of oxides, *J. Vac. Sci. Technol. A*, 1991, **9**, 1793–1805.

48 G. Lucovsky, J. L. Whitten and Y. Zhang, A molecular orbital model for the electronic structure of transition metal atoms in silicate and aluminate alloys, *Solid-State Electron.*, 2002, **46**, 1687–1697.

49 M. J. Guittet, J. P. Crocombette and M. Gautier-Soyer, Bonding and XPS chemical shifts in $ZrSiO_4$ versus SiO_2 and ZrO_2: Charge transfer and electrostatic effects, *Phys. Rev. B*, 2001, **63**, 125117.

50 H. Znad, M. H. Ang, M. O. Tade, Ta/TiO_2-and Nb/TiO_2-Mixed Oxides as Efficient Solar Photocatalysts: Preparation, Characterization, and Photocatalytic Activity, *Int. J. Photoenergy*, 2012, 548158.

51 J. Wang, Y. Yu, S. Li, L. Guo, E. Wang and Y. Cao, Doping Behavior of Zr^{4+} Ions in Zr^{4+}-Doped TiO_2 Nanoparticles, *J. Phys. Chem. C*, 2013, **117**, 27120–27126.

52 P. Babelon, A. S. Dequiedt, H. Mostéfa-Sba, S. Bourgeois, P. Sibillot and M. Sacilotti, SEM and XPS studies of titanium dioxide thin films grown by MOCVD, *Thin Solid Films*, 1998, **322**, 63–67.

53 J. Yan, Y. Kuo and J. Lu, Zirconium-Doped Hafnium Oxide High-k Dielectrics with Subnanometer Equivalent Oxide Thickness by Reactive Sputtering, *Electrochem. Solid-State Lett.*, 2007, **10**, H199–H202.

54 Y. Kuo, J. Lu, J. Yan, T. Yuan, H. C. Kim, J. Peterson, M. Gardner, S. Chatterjee and W. Luo, Mixed Oxide High-k Gate Dielectrics - Interface Layer Structure, Breakdown Mechanism, and Memories, *ECS Trans.*, 2006, **1**, 447–454.

55 D. Barreca, A. Milanov, R. A. Fischer, A. Devi and E. Tondello, Hafnium oxide thin film grown by ALD: An XPS study, *Surf. Sci. Spectra*, 2007, **14**, 34.

56 L. Armelao, S. Gross, E. Tondello and A. Zattin, HfO_2–ZrO_2 Doped Silica Thin Films by XPS, *Surf. Sci. Spectra*, 2003, **10**, 157–163.

57 A. Sinhamahapatra, J.-P. Jeon, J. Kang, B. Han and J.-S. Yu, Oxygen-Deficient Zirconia (ZrO_{2-x}): A New Material for Solar Light Absorption, *Sci. Rep.*, 2016, **6**, 27218.

58 J. Lu and Y. Kuo, Hafnium-doped tantalum oxide high-dielectrics with sub-2 nm equivalent oxide thickness, *Appl. Phys. Lett.*, 2005, **87**, 232906.

59 J. Lu, Y. Kuo and J.-Y. Tewg, Hafnium-Doped Tantalum Oxide High-k Gate Dielectrics, *J. Electrochem. Soc.*, 2006, **153**, G410–G416.

60 E. Atanassova, G. Tyuliev, A. Paskaleva, D. Spassov and K. Kostov, XPS study of N_2 annealing effect on thermal Ta_2O_5 layers on Si, *Appl. Surf. Sci.*, 2004, **225**, 86–99.

61 J. P. Chang, M. L. Steigerwald, R. M. Fleming, R. L. Opila and G. B. Alers, Thermal stability of Ta_2O_5 in metal–oxide–metal capacitor structures, *Appl. Phys. Lett.*, 1999, **74**, 3705–3707.

62 B. Arkles, Silanes and Surfaces: Hydrophobicity, Hydrophilicity and Coupling Agents, in *Silicon Compounds: Silanes & Silicones*, Edited B. Arkles and G. Larson, GELEST (3rd edition), 2013, 119–166.

63 E. Finocchio, E. Macis, R. Raiteri and G. Busca, Adsorption of Trimethoxysilane and of 3-Mercaptopropyltrimethoxysilane on Silica and on Silicon Wafers from Vapor Phase: An IR Study, *Langmuir*, 2007, **23**, 2505–2509.

64 Ch. Weigel and R. Kellner, FTIR-ATR-spectroscopic investigation of the silanization of germanium surfaces with 3-aminopropyltriethoxysilane, *Fresenius Z. Für Anal. Chem.*, 1989, **335**, 663–668.

65 N. Aissaoui, L. Bergaoui, J. Landoulsi, J.-F. Lambert and S. Boujday, Silane Layers on Silicon Surfaces: Mechanism of Interaction, Stability, and Influence on Protein Adsorption, *Langmuir*, 2012, **28**, 656–665.

66 S. Tardio and P. J. Cumpson, Practical estimation of XPS binding energies using widely available quantum chemistry software*, Surf. Interface Anal.*, 2018, **50**, 5–12.

67 M. Giesbers, A. T. M. Marcelis and H. Zuilhof, Simulation of XPS C1s Spectra of Organic Monolayers by Quantum Chemical Methods, *Langmuir*, 2013, **29**, 4782–4788.

68 S. Xiao, P. Xu, Q. Peng, J. Chen, J. Huang, F. Wang and N. Noor, Layer-by-Layer Assembly of Polyelectrolyte Multilayer onto PET Fabric for Highly Tunable Dyeing with Water Soluble Dyestuffs, *Polymers*, 2017, **9**, 735.

69 M. Bengamra, A. Khlifi, N. Ktari, S. Mahouche-Chergui, B. Carbonnier, N. Fourati, R. Kalfat and M. M. Chehimi, Silanized Aryl Layers through Thiol-Yne Photo-Click Reaction. *Langmuir* 2015, **31**, 10717–10724.

70 S. Gam-Derouich, A. Lamouri, C. Redeuilh, P. Decorse, F. Maurel, B. Carbonnier, S. Beyazıt, G. Yilmaz, Y. Yagci and M. M. Chehimi, Diazonium Salt-Derived 4-(Dimethylamino)Phenyl Groups as Hydrogen Donors in Surface-Confined Radical

Photopolymerization for Bioactive Poly(2-Hydroxyethyl Methacrylate) Grafts, *Langmuir* 2012, **28**, 8035–8045.

Surface silanization of equimolar HfNbTaTiZr high-entropy alloy: a first step toward bio-implant applications

M. Gueye[1,2,3], S. Ammar-Merah[2,*], S. Nowak[2], P. Decorse[2], A. Chevillot[2], L. Perrière[3], J. P. Couzinie[3], I. Guillot[3], G. Dirras[1,*]